Journal of Solid State Chemistry 181 (2008) 2789–2795

Contents lists available at ScienceDirect

Journal of Solid State Chemistry

journal homepage: www.elsevier.com/locate/jssc

Crystal growth and structural investigation of A_2BReO_6 (A = Sr, Ba; B = Li, Na)

M. Bharathy, H.-C. zur Loye *

Department of Chemistry and Biochemistry, University of South Carolina, Columbia, SC 29208, USA

ARTICLE INFO

Article history:
Received 21 March 2008
Received in revised form
20 June 2008
Accepted 26 June 2008
Available online 5 July 2008

Keywords:
A_2BReO_6
Double perovskite rhenates
Crystal growth
Hydroxide fluxes

ABSTRACT

Single crystals of the double perovskite rhenates A_2BReO_6 (A = Sr, Ba; B = Li, Na) were grown out of molten hydroxide fluxes. Single crystals of orange/yellow Ba_2LiReO_6, Ba_2NaReO_6 and Sr_2LiReO_6 were solved in the cubic, Fm-3m space group with $a = 8.1214(11)$ Å, 8.2975(3) Å, and 7.9071(15) Å, respectively, while Sr_2NaReO_6 was determined to be monoclinic $P2_1/n$ with $a = 5.6737(6)$ Å, $b = 5.7988(6)$ Å, $c = 8.0431(8)$ Å, and $\beta = 90.02(6)^\circ$. The cubic structure consists of a rock salt lattice of corner-shared ReO_6 and MO_6 (M = Li, Na) octahedra which, in the monoclinic structure, are both tilted and rotated. A discrepancy exists between the symmetry of Sr_2LiReO_6 indicated by the single-crystal refinement of flux-grown crystals (cubic, Fm-3m) and the symmetry indicated by the powder diffraction data collected on polycrystalline samples prepared by the ceramic method (tetragonal, $I4/m$). It is possible that the cubic crystals are a kinetic product that forms in small quantities at low temperatures, while the powder represents the more stable polymorph that forms at higher reaction temperature.

1. Introduction

The perovskite family of oxides has been widely investigated for its ability to accommodate virtually every element in the periodic table as well as for the great variety of properties exhibited by its members that have resulted in their applications in the areas of photocatalysis [1], combustion of methane [2], magnetic refrigerants [3], and magnetic devices [4,5]. Many different synthetic routes have been used for the preparation of perovskite oxides, including the traditional ceramic method [6–8], *chimie douce* [9], combustion methods [10], and low-temperature methods [11], which include hydrothermal synthesis [12], sol gel method [13], metathesis [14], and flux growth [15]. The latter approach has been used extensively by our research group to grow single crystals of double perovskites containing late transition metals, such as Ln_2NaRuO_6 (Ln = La, Pr, Nd) [16], Ln_2LiIrO_6 (Ln = La, Pr, Nd, Sm, Eu) [17], Ba_2MOsO_6 (M = Li, Na) [18], Sr_2NiOsO_6 [19], Ca_2NiOsO_6 [19], Ln_2NaOsO_6 (Ln = La, Pr, Nd) [20], and Ln_2LiOsO_6 (Ln = La, Pr, Nd, Sm) [21] from molten hydroxide fluxes.

The double perovskites rhenates, A_2BReO_6, such as Ba_2MnReO_6 [22], A_2FeReO_6 (A = Ca, Sr, Ba) [23,24], $Ba_2(B/Re)_2O_6$ (B = Fe, Mn, Co and Ni) [25], Sr_2CrReO_6 [26], $Sr_2Fe_{0.9}Sc_{0.1}ReO_6$ [27], and Ba_2LnReO_6 [28] have been widely studied for their physical properties. Among this group, however, the alkali metal containing rhenates are not well represented, although the first syntheses of A_2BReO_6 (A = Ca, Ba, Sr; B = Li, Na) were carried out by Sleight et al. [29,30] many years ago. Subsequent work using hydrothermal methods led to the preparation of Ba_2NaReO_6, which was characterized by single crystal X-ray diffraction [31]. The structural characterization of the analogous strontium-containing members, however, has not been reported. In this paper we report on the crystal growth of A_2BReO_6 (A = Sr, Ba; B = Li, Na) using reactive hydroxide fluxes contained in silver tubes and silver crucibles, as well as the preparation of polycrystalline samples via the ceramic method. Their structure determination and the formation of polymorphs are described herein.

2. Experimental section

2.1. Materials

NH_4ReO_4 (Engelhard Corporation, 99.5%), Re (First Reaction, 99.99%) $Ba(OH)_2 \cdot 8H_2O$ (Alfa Aesar, 98%), $Sr(OH)_2$ (Aldrich, 96%), $LiOH \cdot H_2O$ (Alfa Aesar, 99.9%), and NaOH (Alfa Aesar, 99.5%) were used as received.

2.2. Crystal growth

Single crystals of A_2BReO_6 (A = Sr, Ba; B = Li, Na) were grown from reactive hydroxide fluxes, where NH_4ReO_4 and/or Re metal were used as rhenium sources. Yellowish crystals of A_2BReO_6

* Corresponding author. Fax: +1 803 777 8508.
E-mail address: zurloye@mail.chem.sc.edu (H.-C. zur Loye).

0022-4596/$ - see front matter © 2008 Elsevier Inc. All rights reserved.
doi:10.1016/j.jssc.2008.06.056

(A = Sr, Ba; B = Li, Na) were grown from NH_4ReO_4 (0.2658 g, 1 mmol), or Re metal (0.1862 g, 1 mmol), $A(OH)_2$ (0.5 g), and BOH (3 g) in silver tubes that were flame sealed at one end. The other end of the filled tubes was crimped and folded twice before being placed upright into a programmable furnace. The filled silver tubes were heated to a reaction temperature of 700 or 750 °C at 600 °C/h. All reactions were held at either 700 or 750 °C for 12 h, slowly cooled to 600 °C at 5 °C/h, and then cooled to room temperature by shutting off the furnace. The crystal quality was typically better for reactions carried out at 750 °C; however, at that temperature the product yield was reduced. The crystals were isolated by dissolving the flux with methanol, aided by sonication. Note: washing the samples with water leads to severe crystal degradation.

2.3. Powder synthesis

Solid-state syntheses of A_2BReO_6 (A = Sr, Ba; B = Li, Na) were carried out using stoichiometric quantities of ACO_3, B_2CO_3 (A = Sr, Ba; B = Li, Na), and rhenium metal. The thoroughly ground starting materials were placed in alumina boats as powders and heated at 900 °C for 4 h in air. The reaction mixtures after the first heating cycle were again ground and further sintered at 1050, 1000, and 1100 °C for 12 h to obtain pure phases of Sr_2LiReO_6, Ba_2LiReO_6, and Ba_2NaReO_6 respectively. A pure phase of Sr_2NaReO_6 could not be obtained and the samples always contained Re_2O_7 as an impurity phase.

2.4. Scanning electron microscopy

Scanning electron micrographs of single crystals were obtained using a FEI Quanta SEM instrument operated in the low-vacuum mode. A representative image of a Ba_2NaReO_6 crystal to illustrate the crystal morphology is shown in Fig. 1. Energy-dispersive spectroscopy verified the presence of Sr, Ba, Na, and Re within the detection limits of the instrument and confirmed the absence of extraneous elements, such as silver.

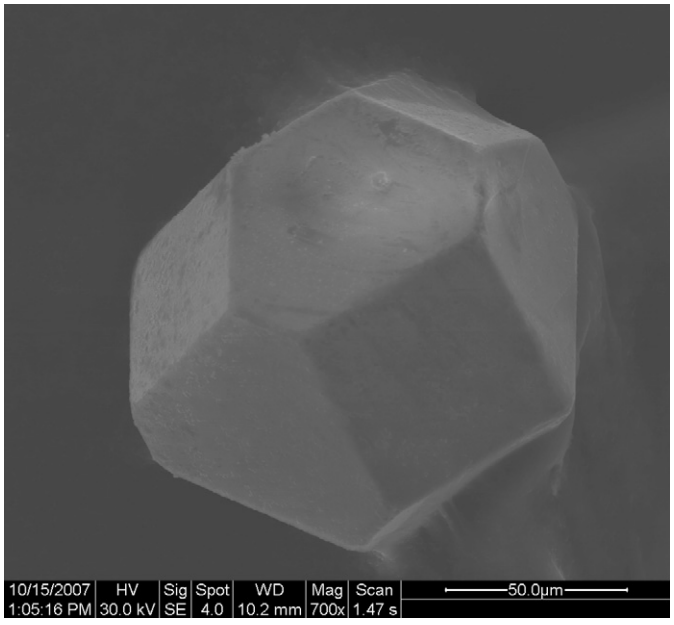

Fig. 1. SEM image of a single crystal of Ba_2NaReO_6.

2.5. ICP elemental analysis

The presence of lithium in Sr_2LiReO_6 and Ba_2LiReO_6 was verified by ICP analysis performed by Desert Analytics Corporation. Analysis Calculated for Sr_2LiReO_6: Li, 1.4%; found: Li, 1.1%. Analysis calculated for Ba_2LiReO_6: Li, 1.2%; Found: Li, 1.2%).

2.6. Optical properties

The UV–visible diffuse reflectance spectra of A_2BReO_6 (A = Sr, Ba; B = Li, Na) were obtained on a Perkin-Elmer Lambda 35 UV–visible spectrophotometer equipped with an integration sphere.

2.7. ^{7}Li NMR spectroscopy

^{7}Li NMR spectra were recorded on ground samples of Sr_2LiReO_6 and Ba_2LiReO_6 on a Varian Inova 500 NMR spectrometer. The samples were loaded on a 4 mm mass probe and spun at 10 kHz. LiCl was used as reference.

2.8. Single crystal X-ray diffraction

Single crystal X-ray diffraction data for A_2BReO_6 (A = Sr, Ba; B = Li, Na) were collected on a Bruker SMART APEX CCD-based diffractometer with a crystal-to-detector distance of 5.016 cm using monochromated Mo $K\alpha$ radiation. A complete sphere of reciprocal space was covered with different φ angles (φ = 0, 90, 180 and 0°) based on four sets of runs. Each frame covered 0.3° in ω. The data were integrated using *SAINTPLUS* [32]. An empirical absorption correction was applied in each case. The structures were solved by direct methods with SHELXS97 [33] and refined using SHELXL97 [34]. The structures of Ba_2LiReO_6, Ba_2NaReO_6, and Sr_2LiReO_6, were solved in the cubic space group Fm-3m, while the structure of Sr_2NaReO_6 was solved in the monoclinic space group $P2_1/n$. The heavy atom (Sr/Ba and Re) locations in the crystal structures were obtained by direct methods. Subsequent difference Fourier synthesis revealed (Na/Li), and O atoms in the structures. All atoms were refined with anisotropic displacement parameters.

The refinements of Ba_2LiReO_6, Ba_2NaReO_6, and Sr_2LiReO_6 proceeded without problems; however, the refinement of monoclinic Sr_2NaReO_6 required the inclusion of oxygen positional disorder with partial site occupancies. The initial structure refinement resulted in an R factor of 7% with high thermal parameters on all oxygen atoms. The difference Fourier map revealed residual electron densities of 6 e/Å^3 on atoms O(1), O(2), and O(3), indicating positional disorder. These electron density peaks were assigned as oxygen atoms O(4), O(5), and O(6) and their occupancies were refined, restricting the sums of occupancies at each pair of split oxygen sites (O(1), O(4); O(2), O(5); and O(3), O(6)) to unity. The occupancy refinements indicated partial occupancies of oxygen at each site and the R index dropped to ~5% with negligible electron density (~1.31 e/Å^3) around the oxygen atoms. No deviation from unity occupancy was observed for either of the heavy atoms. The atomic coordinates are listed in the supplementary information. Crystallographic data and details of the single crystal data collection of A_2BReO_6 (A = Sr, Ba; B = Li, Na) are given in Tables 1a and 1b. Table 2 lists the atomic coordinates of all the four oxides.

2.9. Powder X-ray diffraction

Powder X-ray diffraction patterns were collected on a Rigaku Dmax/2100 powder diffractometer using Cu $K\alpha$ radiation. Data for

Table 1a
Crystallographic data of Sr_2LiReO_6 and Sr_2NaReO_6

Empirical formula	Sr_2LiReO_6	Sr_2NaReO_6
Crystal habit, color	Hexagonal, yellow	Hexagonal, orange
Crystal size (mm^3)	$0.023 \times 0.015 \times 0.009$	$0.1 \times 0.05 \times 0.04$
Crystal system	Cubic	Monoclinic
Space group	*Fm*-3*m*	$P2_1/n$
Cell dimensions		
a (Å)	7.9071(15)	5.6737(6)
b (Å)		5.7988(6)
c (Å)		8.0431(8)
β (deg)		90.02(6)
Volume ($Å^3$)	494.37(16)	264.62(5)
Formula weight	464.37	480.82
D_x (g/cm^3)	6.239	6.035
Z	4	2
F(000)	808	420
θ_{max} (deg)	35.63	36.08
Recording reciprocal space	$-12 \leqslant h \leqslant 12$, $-11 \leqslant k \leqslant 12$, $-12 \leqslant l \leqslant 5$	$-9 \leqslant h \leqslant 7$, $-9 \leqslant k \leqslant 9$, $-13 \leqslant l \leqslant 9$
Number of measured reflections	1320	2701
Number of independent reflections	84 With $I > 3\sigma(I)$ [R(int) = 0.0313]	1199 With $I > 3\sigma(I)$ [R(int) = 0.0323]
μ (mm^{-1})	45.87	42.938
Refinement	F^2	F^2
No. of variables	7	76
$R(F)$	0.0246	0.0498
$wR(F^2)$	0.0639	0.1478
GoF	0.969	1.21
Max./min. $\Delta\rho$ ($e/Å^3$)	0.999/−1.10	1.431/−2.38

Table 1b
Crystallographic data of Ba_2LiReO_6 and Ba_2NaReO_6

Empirical formula	Ba_2LiReO_6	Ba_2NaReO_6
Crystal habit, color	Hexagonal, yellow	Hexagonal, yellow
Crystal size (mm^3)	$0.02 \times 0.01 \times 0.008$	$0.031 \times 0.02 \times 0.009$
Crystal system	Cubic	Cubic
Space group	*Fm*-3*m*	*Fm*-3*m*
Cell dimensions		
a (Å)	8.1214(11)	8.2975(3)
Volume ($Å^3$)	535.66(13)	571.27(4)
Formula weight	563.817	579.85
D_x (g/cm^3)	6.991	6.742
Z	4	4
F(000)	952	984
θ_{max} (deg)	29.67	35.85
Recording reciprocal space	$-3 \leqslant h \leqslant 11$, $-11 \leqslant k \leqslant 11$, $-11 \leqslant l \leqslant 11$	$-9 \leqslant h \leqslant 13$, $-13 \leqslant k \leqslant 8$, $-9 \leqslant l \leqslant 13$
Number of measured reflections	831	878
Number of independent reflections	105 With $I > 3\sigma(I)$ [R(int) = 0.0546]	92 With $I > 3\sigma(I)$ [R(int) = 0.0323]
μ (mm^{-1})	37.036	34.807
Refinement	F^2	F^2
No. of variables	7	7
$R(F)$	0.0434	0.0352
$wR(F^2)$	0.0889	0.0906
GoF	0.896	0.823
Max./min. $\Delta\rho$ ($e/Å^3$)	0.999/−2.21	1.431/−2.38

polycrystalline samples were collected and *Le Bail* profile fits were performed using *JANA*2000 [35] to confirm the purity of the samples in each case. The *Le Bail* profile fits and details of refinement of Ba_2NaReO_6 and Ba_2LiReO_6 are shown in Supplementary Information (Figures S1, S2 and Table S1). The data for Sr_2LiReO_6 were also used to perform a Rietveld refinement to confirm the tetragonal structure of the polycrystalline sample. The data for the Rietveld refinement were collected over the two-theta range of 5° to 80° using a step size of 0.05°. The lattice parameters, atomic positions, and thermal parameters were refined. The background was modeled using the Chebyshev polynomial. The peak shapes were modeled using a pseudo-Voigt function. Crystallographic data and details of the Rietveld refinement are given in Table 3.

Table 2
Atomic coordinates and equivalent isotropic displacement parameters for Sr_2LiReO_6, Sr_2NaReO_6, Ba_2LiReO_6, and Ba_2NaReO_6

	x	*y*	*z*	Occupancy	U_{eq}
Sr_2LiReO_6				1	
Sr(1)	0.25	0.25	0.25	1	0.0117(3)
Li(1)	0	0.5	0	1	0.030(14)
Re(1)	0	0	0	1	0.0064(2)
O(1)	0	0.2358(10)	0	1	0.0279(19)
Sr_2NaReO_6					
Sr(1)	0.5006(2)	0.0448(2)	0.24836(14)	1	0.0141(2)
Na(1)	0	0	−0.5	1	0.0182(17)
Re(1)	0	0	0	1	0.00787(16)
O(1)	0.074(4)	0.022(4)	−0.224(2)	0.39(1)	0.013(4)
O(2)	0.261(3)	−0.184(4)	0.038(2)	0.43(2)	0.011(3)
O(3)	0.176(3)	0.261(3)	0.0458(18)	0.50(1)	0.010(3)
O(4)	−0.076(3)	0.030(3)	−0.227(3)	0.62(1)	0.027(3)
O(5)	0.178(3)	−0.273(4)	−0.043(3)	0.50(1)	0.021(4)
O(6)	0.265(3)	0.183(3)	−0.031(3)	0.57(2)	0.026(4)
Ba_2LiReO_6					
Ba(1)	0.25	0.25	0.25	1	0.0082(6)
Li(1)	0	0	0	1	0.020(15)
Re(1)	0.5	0	0	1	0.0091(7)
O(1)	0.2681(13)	0	0	1	0.0108(17)
Ba_2NaReO_6					
Ba(1)	0.25	0.25	0.25	1	0.0093(4)
Na(1)	0	0	0	1	0.011(3)
Re(1)	0.5	0.5	0.5	1	0.0049(3)
O(1)	0.2753(7)	0	0	1	0.0146(13)

Table 3
Rietveld refinement data for Sr_2LiReO_6

Empirical formula	Sr_2LiReO_6
Crystal system	Tetragonal
Space group	*I*4/*m*
Cell dimensions	
a (Å)	5.5467(2)
c (Å)	7.9197(4)
Volume ($Å^3$)	244.289(11)
No. of reflections	1512
No. of parameters	43
R_p	0.151
R_{wp}	0.198
R_{exp}	0.067
R_{bragg}	0.080

3. Results and discussion

3.1. Crystal structures of A_2BReO_6 (A = Sr, Ba; B = Li, Na)

The ideal ABO_3 perovskite structure is cubic with the *A*-cation located in a 12-fold and the *B*-cation in a six-fold coordination environment and forms when the radii of the *A* and *B* cations fall into a specific size regime. If the *A*-cation is small, relative to *B* and O, then the structure distorts by a process that involves a combination of tilting and rotation of the BO_6 octahedra, and the cubic symmetry is lost. This is true for the simple ABO_3 perovskite, as well as for the $A_2BB'O_6$ double perovskite. The likelihood of a distortion for a specific cation size is indicated by the Goldschmidt tolerance factor [36] *t*, defined by $t = (r_A + r_O)/\sqrt{2}(r_B + r_O)$, where r_A, r_B, and r_O are the ionic radii of the respective ions. For $t \sim 1$, the perovskite structure is expected to be cubic, while for smaller

values of t, the structure distorts and becomes tetragonal or monoclinic. To determine t for double perovskites, $A_2BB'O_6$, $r_{BB'}$, the average value of r_B and $r_{B'}$ is used instead of r_B, and the equation changes to $t = (r_A + r_O)/\sqrt{2}(\bar{r}_{BB'} + r_O)$.

Based on this equation, and using the oxidation state specific ionic radii compiled by Shannon and Prewitt [37], the room temperature tolerance factors for Sr_2LiReO_6, Sr_2NaReO_6, Ba_2LiReO_6 and Ba_2NaReO_6, are 0.98, 0.92, 1.04, and 0.98, respectively. We can use these values in a somewhat predictive manner, since, in general, perovskites with tolerance factors in the range 0.98–1.07 crystallize into the cubic *Fm*-3*m* space group, while those in the range 0.97–0.99 crystallize into the tetragonal *I*4/*m* space group [38]. Compositions with even smaller tolerance factors (0.86–0.97) are typically monoclinic [38,39]. Thus, we would expect Ba_2LiReO_6, Ba_2NaReO_6 and Sr_2LiReO_6, to crystallize in the cubic *Fm*-3*m* system, and Sr_2NaReO_6 in the monoclinic $P2_1/n$ system. These symmetry predictions were confirmed for all but Sr_2LiReO_6, which proved contentious in that the single crystal analysis indicated a cubic *Fm*-3*m* system, while the Rietveld analysis of the polycrystalline powder indicated the tetragonal *I*4/*m* system.

Compounds that have tolerance factors close to structure boundaries, however, often surprise us. Thus, Ba_2CuTeO_6 [40] (t~1.042) and Ba_2WCuO_6 [41] (t~1.042) crystallize in the tetragonal *I*4/*m* system, despite tolerance factors greater than unity. In our case, Sr_2LiReO_6 with tolerance factor $t = 0.98$ crystallizes very close to the cubic *Fm*-3*m*/tetragonal *I*4/*m* border, and its single crystal structure refines as cubic and its polycrystalline powder structure as tetragonal. It is worth noting that a majority of strontium-containing double perovskites with tolerance factors in the range of 0.98–0.99 crystallize in the tetragonal *I*4/*m*, rather than in the cubic *Fm*-3*m*, space group [38].

3.2. Ba_2LiReO_6 and Ba_2NaReO_6

Yellow/orange crystals of A_2BReO_6 (A = Ba; B = Li, Na) were grown from molten hydroxide fluxes in sealed silver tubes, where the flux acted as both melt and reactant. A preliminary structure analysis by powder X-ray diffraction indicated the formation of the cubic form of the double perovskite, which was confirmed by single crystal X-ray diffraction. Ba_2LiReO_6 and Ba_2NaReO_6 crystallize in the cubic crystal system, *Fm*-3*m*, with $a = 8.1214(11)$ Å and $a = 8.2975(3)$ Å, respectively. The lattice parameters and coordinates of Ba_2NaReO_6 are in agreement with the earlier report [31]. The crystal structures of these two double perovskites, shown in Fig. 2a, consist of a rock salt lattice of corner-shared BO_6 (Na, Li) and ReO_6 octahedra, with barium occupying the 12-fold coordination environment located at the center of a cube of eight corner-shared octahedra. The alkali metal and the rhenium cations are located on alternating octahedral sites in the structure, where the large difference in their oxidation states (+1/+7) drives the charge ordering. The Re–O bond distances in Ba_2LiReO_6, 1.883(11) Å, are slightly longer than those in the sodium analog, Ba_2NaReO_6, 1.865(6) Å, similar to the trend observed for the isostructural

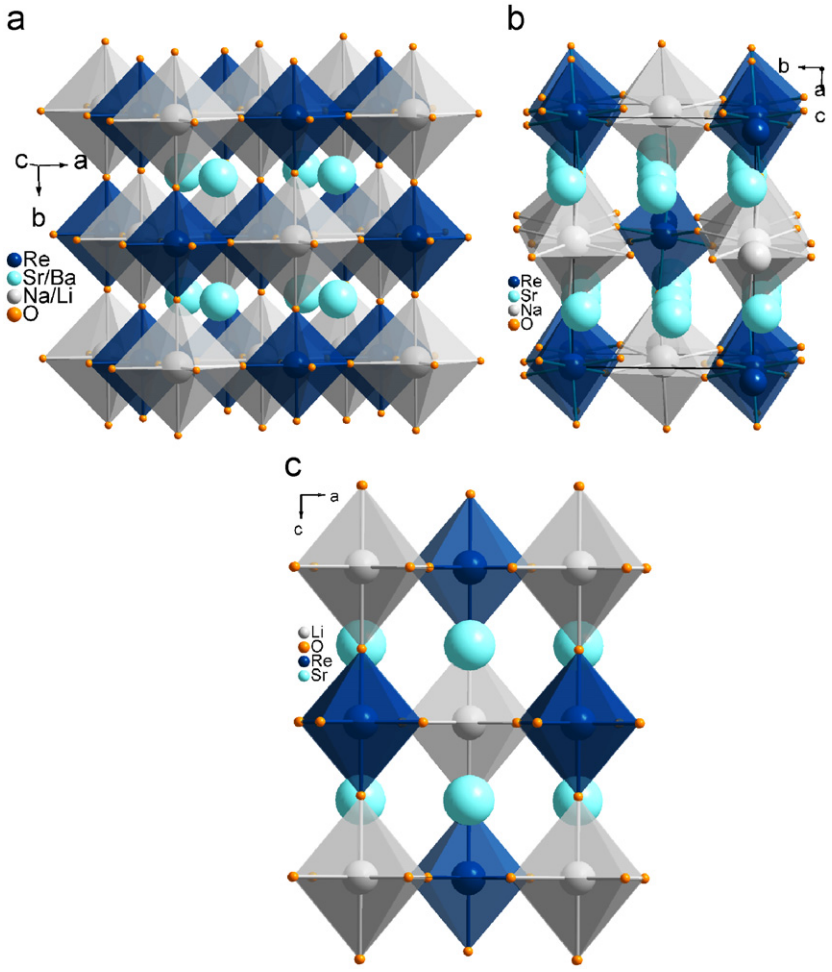

Fig. 2. Single-crystal structures of (a) Ba_2NaReO_6, Sr_2LiReO_6 and Ba_2LiReO_6. (b) Sr_2NaReO_6 (disordered oxygen atoms are omitted for clarity). (c) Crystal structure of Sr_2LiReO_6 based on powder X-ray diffraction data. The octahedra in all cases are corner shared with each other.

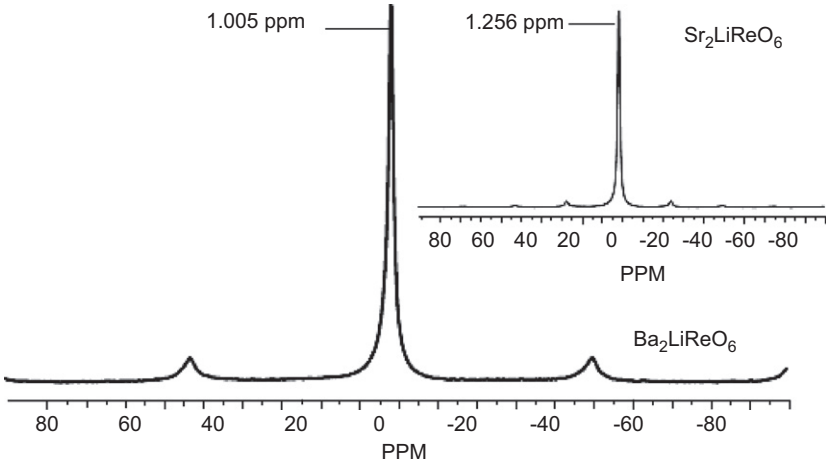

Fig. 3. Solid-state ^{7}Li NMR spectra of Sr_2LiReO_6 and Ba_2LiReO_6 (inset).

osmates, Ba_2LiOsO_6 and Ba_2NaOsO_6 [18]. Furthermore, the Li–O and Na–O bond distances in Ba_2LiReO_6 and Ba_2NaReO_6 are in good agreement with the values reported for the isostructural osmates [18].

Because lithium is a light atom that is difficult to refine in the presence of the heavier barium and rhenium atoms, we performed solid-state ^{7}Li NMR studies to confirm the presence of lithium in Ba_2LiReO_6. The NMR spectrum, shown in inset to Fig. 3, consists of a central band flanked by side bands generated by first-order quadrupolar coupling. Similar ^{7}Li NMR results were obtained for Sr_2LiReO_6 (Fig. 3).

3.3. Sr_2NaReO_6

Yellow/orange crystals of Sr_2NaReO_6 were grown from molten hydroxide fluxes in sealed silver tubes, where the flux acted as both melt and reactant. A preliminary structure analysis by powder X-ray diffraction indicated the formation of the monoclinic form of the double perovskite, which was confirmed by single crystal X-ray diffraction. The single crystal structure of Sr_2NaReO_6 was refined in the monoclinic space group $P2_1/n$ system with $a = 5.6737(6)$ Å, $b = 5.7988(6)$ Å, $c = 8.0431(8)$ Å, and $\beta = 90.02(6)^\circ$. To obtain a satisfactory structure refinement, oxygen disorder had to be included in the structure solution. The structure is shown in Fig. 2b and consists of a distorted rock salt framework of corner-shared NaO_6 and ReO_6 octahedra, with strontium occupying an eight fold coordination environment in the middle of eight corner-shared NaO_6 and ReO_6 octahedra. The Re–O bond distances are in the range 1.849(16)–1.91(2) Å. The distortion from the ideal perovskite structure results from the tilting of the NaO_6 and ReO_6 octahedra to accommodate the strontium cation. There is considerable distortion in the Na–O–Re bond angle from the ideal value of 180° to 155°, indicating the degree of structural distortion.

3.4. Sr_2LiReO_6

3.4.1. Single crystal structure

Yellow/orange crystals of Sr_2LiReO_6 were grown from molten hydroxide fluxes in sealed silver tubes, where the flux acted as both melt and reactant. The single crystal X-ray diffraction data for Sr_2LiReO_6 were refined as cubic in the space group $Fm\text{-}3m$, with $a = 7.9071(15)$ Å. This was unexpected, since the preliminary powder X-ray diffraction data had indicated a tetragonal structure with unit cell parameters $a = 5.5467(2)$ Å and $c = 7.9197(4)$ Å. Forcing the single crystal X-ray data into the tetragonal $I4/m$ system yielded a structure with lattice parameters $a = 5.5030(9)$ Å and $c = 7.7567(25)$ Å; however, this did not turn out to be a satisfactory structure solution. The ReO_6 octahedra in the tetragonal solution of Sr_2LiReO_6 exhibited axial elongation, as manifested by the slight variations in the Re–O bond distances (1.82(4)–1.84(1) Å). The poor standard deviations for bond distances Re–O (1.82(4) Å) and Li–O (2.06(4) Å) and a high R factor (~0.06) suggest that the cubic structural model is the best fit for the single crystals. Because the yield of cubic crystals was very poor, we were unable to collect enough single crystals to crush and use for powder X-ray diffraction. Eight crystals from different batches were analyzed by single crystal X-ray diffraction and all were found to be cubic. The Re–O and Sr–O bond distances obtained from the cubic refinement are 1.864(8) and 2.7978(6) Å, respectively.

3.4.2. Polycrystalline powder structure

To confirm the tetragonal symmetry of the polycrystalline powder of Sr_2LiReO_6, we fitted the data using the Rietveld method in the tetragonal space group $I4/m$. The starting structural model for the tetragonal symmetry was taken from SPuDS [42], which provided estimated lattice parameters and atomic positions. The refinement quickly converged on refinement of the lattice parameters and the atomic coordinates (Fig. 4). We fixed the atomic coordinates of the lithium using the SPuDS coordinates, as it is not reliable to refine such a light atom in the presence of heavy atoms when using laboratory X-ray diffraction data. The Re–O bond distances (1.8753(1) and 1.8889(1) Å) obtained from this refinement agreed well with those obtained from the single crystal data discussed above. Furthermore, electron diffraction data (collected on a Hitachi H8000 Scanning Transmission Electron Microscope) on the polycrystalline portion from flux synthesis clearly indicated tetragonal symmetry consistent with the powder X-ray data.

3.5. Polymorphism of Sr_2LiReO_6

The crystal growth of Sr_2LiReO_6 resulted in the formation of a modest amount of cubic crystals with the vast majority of product consisting of polycrystalline powder. The polycrystalline powder was indexed as tetragonal in the powder X-ray diffraction analysis, while the crystals were determined to be cubic by single crystal X-ray diffraction. To explain the formation of both cubic crystals and tetragonal polycrystalline powder, we propose that the cubic crystals are a kinetic product that forms in small quantities at low temperatures, while the powder represents the

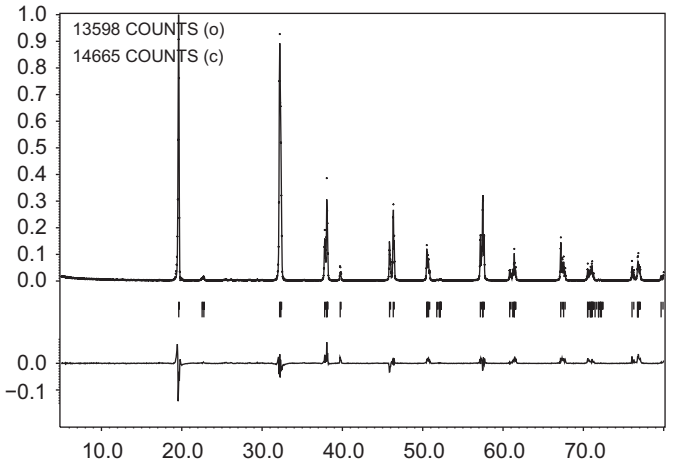

Fig. 4. Rietveld refinement fit of Sr_2LiReO_6. Collected data are represented by stars (*) while the solid lines represent the fit. A difference plot between the observed and calculated intensities is shown below. Tick marks indicate allowed reflections in the space group $I4/m$.

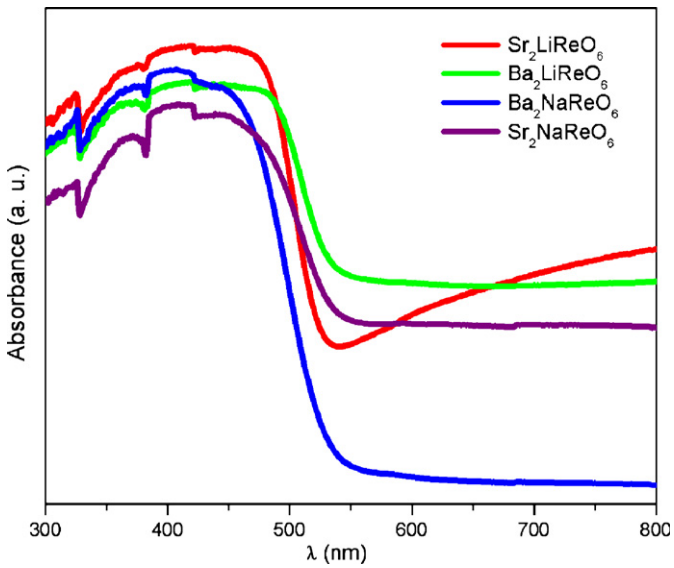

Fig. 5. UV–visible spectra of A_2BReO_6 (A = Sr, Ba; B = Li, Na).

more stable polymorph that forms at the higher reaction temperature. This is consistent with the fact that a solid-state synthesis results in the tetragonal polymorph.

Another possibility worth considering is the preferential loss of lithium during the ceramic synthesis. In that case, the change in symmetry may be due to a lithium deficiency in the sample. On the other hand, polycrystalline Sr_2LiReO_6 synthesized by the flux method, (where it is less likely that any lithium loss would take place) also has tetragonal symmetry, arguing against this possibility. ICP analysis, although consistent with the formula, is not accurate enough to reveal the small lithium deficiencies in the sample. Hence, establishing the precise lithium content of the samples is extremely difficult.

Varying the heating and cooling profile did not result in improved yields of single crystals and only when the samples were heated to 750 °C were good quality single crystals obtained. The quality of the polycrystalline product was also sensitive to the reaction conditions and deteriorated when the cooling rate was decreased. Interestingly, the best products were obtained for a slow cooling step from 750 to 650 °C, while only poorly crystalline products were obtained for a more extensive slow cooling from 750 to 300 °C.

To investigate if tetragonal Sr_2LiReO_6 undergoes a phase transition on heating, DTA/TG analyses were performed on it and on the other A_2BReO_6 (A = Sr, Ba; B = Li, Na) compositions. There was no indication in the DTA data that any of these compositions undergo a structural transition as a function of temperature. Finally, on heating samples to 1100 °C and higher, Sr_2LiReO_6, Sr_2NaReO_6, and Ba_2LiReO_6 undergo transformation to the fluorite-related $A_5Re_2O_{12}$ (A = Ba, Sr) structure type. Ba_2NaReO_6 alone is stable up to 1200 °C, the limits of our measurement.

It is known that some double perovskites undergo a phase transition to lower symmetry on cooling. Since it appears that Sr_2LiReO_6 is close to a cubic/tetragonal phase transition we explored the possibility of a low-temperature structure transition in Sr_2LiReO_6 and collected a low-temperature data set on the cubic single crystals at 100 K. It also was found to be cubic, indicating that the cubic phase, once formed, is stable down to 100 K.

3.6. Optical properties

The UV–visible absorbance spectra of A_2BReO_6 (A = Sr, Ba; B = Li, Na) are shown in Fig. 5. The measurements were made on powder samples consisting of ground single crystals of Ba_2LiReO_6, Ba_2NaReO_6, and Sr_2NaReO_6, while in the case of Sr_2LiReO_6, polycrystalline powders were used. Orange crystals of Sr_2NaReO_6 were carefully separated from the Re_2O_7 impurities under an optical microscope prior to grinding. As expected, the measured absorption edges are all similar at 504 nm (2.46 eV), 502 nm (2.47 eV), 508 nm (2.44 eV), and 501 nm (2.47 eV) for Sr_2LiReO_6, Sr_2NaReO_6, Ba_2LiReO_6, and Ba_2NaReO_6, respectively.

4. Conclusion

Single crystals of double perovskite rhenates, A_2BReO_6 (A = Sr, Ba; B = Li, Na), were grown from reactive hydroxide fluxes from sealed silver tubes. Single crystals of Sr_2LiReO_6, Ba_2LiReO_6, and Ba_2NaReO_6 exhibit cubic symmetry, while Sr_2NaReO_6 crystallizes into the monoclinic form. Polycrystalline powders of Sr_2LiReO_6 show tetragonal symmetry. UV–visible spectra indicate similar values of absorption edges for all the phases.

Supplemental information

Further details of the crystal structure investigations can be obtained from the Fachinformationszentrum Karlsruhe, 76344 Eggenstein-Leopoldshafen, Germany (fax: +49 7247 808 666; e-mail: crystdata@fiz-karlsruhe.de) on quoting the depository numbers CSD-18990-418994.

Acknowledgments

Financial support from the National Science Foundation through Grants DMR:0450103 and DMR:0804209 is gratefully acknowledged. We would like to thank Dr. Mark Smith for helpful discussions and for the low-temperature single crystal data collection of Sr_2LiReO_6.

Appendix A. Supporting Information

Supplementary data associated with this article can be found in the online version at doi:10.1016/j.jssc.2008.06.056.

References

[1] B. Xu, W.F. Zhang, X.-Y. Liu, J.H. Ye, W.H. Zhang, L. Shi, X.G. Wan, J. Yin, Z.G. Liu, Phy. Rev. B 76 (2007) 1251091–1251096.
[2] G.-L. Chiarello, I. Rossetti, P. Lopinto, G. Migliavacca, L. Forni, Catal. Today 117 (2006) 549–553.
[3] M.-H. Phan, H.-X. Peng, S.-C. Yu, N.-D. Tho, H.-N. Nhat, N. Chau, J. Magn. Magn. Mater. 316 (2007) e562–e565.
[4] K.-I. Kobayashi, T. Kimura, H. Sawada, K. Terakura, Y. Tokura, Nature 395 (1998) 677–680.
[5] K.-I. Kobayashi, T. Kimura, Y. Tomioka, H. Sawada, K. Terakura, Y. Tokura, Phys. Rev. B 59 (1999) 11159–11162.
[6] N. Taira, Y. Hinatsu, J. Solid State Chem. 150 (2000) 31–35.
[7] D. Li, J. Zheng, Z. Zou, J. Phys. Chem. Solids. 67 (2006) 801–806.
[8] K.L. Holman, Q. Huang, T. Klimczuk, K. Trzebiatowski, J.W.G. Bos, E. Morosan, J.W. Lynn, R.J. Cava, J. Solid State Chem. 180 (2007) 75–83.
[9] J. Gopalakrishnan, Chem. Mater. 7 (1995) 1265–1275.
[10] D.A. Furno, J.R. Jurado, A.M. Segadses, J.R. Frade, Mater. Res. Bull. 32 (1997) 1459–1470.
[11] R.E. Schaak, T.E. Mallouk, Chem. Mater. 14 (2002) 1455–1471.
[12] Y. Chen, H. Yuan, G. Li, G. Tian, S. Feng, J. Cryst. Growth. 305 (2007) 242–248.
[13] S.Z. Tian, J.C. Zhao, C.D. Qiao, X.L. Ji, B.Z. Jiang, Mater. Lett. 60 (2006) 2747–2750.
[14] T.K. Mandal, J. Gopalakrishnan, Chem. Mater. 17 (2005) 2310–2316.
[15] D. Elwell, H.J. Scheel, Crystal Growth from High-Temperature Solutions, Academic Press, New York, 1975.
[16] W.R. Gemmill, M.D. Smith, H.-C. zur Loye, J. Solid State Chem. 177 (2004) 3560–3567.
[17] S.J. Mugavero, M.D. Smith, H.-C. zur Loye, J. Solid State Chem. 178 (2005) 200–206.
[18] K.E. Stitzer, M.D. Smith, H.-C. zur Loye, Solid State Sci. 4 (2002) 311–316.
[19] R. Macquart, S.-J. Kim, W.R. Gemmill, J.K. Stalick, Y. Lee, T. Vogt, H.-C. zur Loye, Inorg. Chem. 44 (2005) 9676–9683.
[20] W.R. Gemmill, M.D. Smith, R. Prozorov, H.-C. zur Loye, Inorg. Chem. 44 (2005) 2639–2646.
[21] W.R. Gemmill, M.D. Smith, H.-C. zur Loye, J. Solid State Chem. 179 (2006) 1750–1756.
[22] C.P. Khattak, D.E. Cox, F.F.Y. Wang, J. Solid State Chem. 13 (1975) 77–83.
[23] J. Gopalakrishnan, A. Chattopadhyay, S.B. Ogale, T. Venkatesan, R.L. Greene, A.J. Millis, K. Ramesha, B. Hannoyer, G. Marest, Phy. Rev. B 62 (2000) 9538–9542.
[24] S.E. Lofland, T. Scabarozi, S. Kale, S.M. Bhagat, S.B. Ogale, T. Venkatesan, R.L. Greene, J. Gopalakrishnan, K. Ramesha, IEEE Trans. Magn. 37 (2001) 2153–2155.
[25] N. Rammeh, H. Ehrenberg, H. Fuess, A. Cheikkh -Rouhou, Phys. Stat. Solidi C 9 (2006) 3225–3228.
[26] H. Kato, T. Okuda, Y. Okimoto, Y. Tomioka, Y. Takenoya, A. Ohkubo, M. Kawasaki, Y. Tokura, Appl. Phys. Lett. 81 (2002) 328–330.
[27] J.J. Blanco, T. Hernandez, M.R.-M. Lide, M. Insausti, J.M. Barandiaran, J.-M. Greneche, T. Rojo, J. Mater. Chem. 11 (2001) 253–256.
[28] Y. Sasaki, Y. Doi, Y. Hinatsu, J. Mater. Chem. 12 (2002) 2361–2366.
[29] A.W. Sleight, R. Ward, J. Am. Chem. Soc. 83 (1961) 1088–1090.
[30] A.W. Sleight, J. Longo, R. Ward, Inorg. Chem. 1 (1962) 245–250.
[31] J.-P. Picard, M. Aneas, G. Baud, J.-P. Besse, R. Chevalier, J. Less Common Metals. 79 (1981) 165–167.
[32] Bruker, SAINT (Version 6.45a), Bruker AXS Inc., Madison, WI, USA, 2000.
[33] G.M. Sheldrick, SHELXS97. Program for Crystal Structure Solution, University of Gottingen, Germany, 1997.
[34] G.M. Sheldrick, SHELXL97. Program for Crystal Structure Refinement, University of Gottingen, Germany, 1997.
[35] V. Petricek, M. Ducek, *JANA2000*, Structure Determination Software Programs, Institute of Physics, Praha, Czech Republic, 2000.
[36] V.M. Goldschmidt, Geochemische Verteilungsgesetze der Elementer V11, Naturvidenskaplig Klasse, Oslo, 1926.
[37] R.D. Shannon, C.T. Prewitt, Acta Crystallogr. B 25 (1969) 925–946.
[38] M.W. Lufaso, P.W. Barnes, P.M. Woodward, Acta Crystallogr. B 62 (2006) 397–410.
[39] Note that another predictive model was developed by Teraoka et al. based on his "fitness hypothesis" Y. Teraoka, M.-D. Wei, S. Dagawa, J. Mater. Chem. 8 (1998) 2323–2325.
[40] D. Iwanaga, Y. Inaguma, M. Itoh, J. Solid State Chem. 147 (1999) 291–295.
[41] Bokhimi, Powder Diffr. 7 (1992) 228–230.
[42] M.W. Lufaso, P.M. Woodward, Acta Crystallogr. B 57 (2001) 725–738.